Magnetic hardening and antiferromagnetic/ferromagnetic phase coexistence in $Mn_{1-x}Fe_xRu_2Sn$ Heusler solid solutions

Jason E. Douglas,* Emily E. Levin, and Tresa M. Pollock
Materials Department, University of California, Santa Barbara, California 93106, USA
and Materials Research Laboratory, University of California, Santa Barbara, California 93106, USA

Juan C. Castillo
Department of Electrical and Computer Engineering, University of California, Santa Barbara, California 93106, USA

Peter Adler and Claudia Felser
Max Planck Institute for Chemical Physics of Solids, D-01187 Dresden, Germany

Stephan Krämer
Materials Department, University of California, Santa Barbara, California 93106, USA

Katharine L. Page
Chemical and Engineering Materials Division, Spallation Neutron Source, Oak Ridge National Laboratory, Oak Ridge, Tennessee 37831, USA

Ram Seshadri
Materials Department, University of California, Santa Barbara, California 93106, USA;
Materials Research Laboratory, University of California, Santa Barbara, California 93106, USA;
and Department of Chemistry and Biochemistry, University of California, Santa Barbara, California 93106, USA
(Received 21 June 2016; revised manuscript received 24 August 2016; published 13 September 2016)

We investigate the average structure, local structure, and magnetic behavior of Heusler alloys of the composition $Mn_{1-x}Fe_xRu_2Sn$, between antiferromagnetic (AFM) $MnRu_2Sn$ and ferromagnetic (FM) $FeRu_2Sn$ (often written Ru_2MnSn and Ru_2FeSn). Using a combination of neutron total scattering, electron microscopy, and ^{57}Fe Mössbauer spectroscopy, we conclude that true solid solutions are formed across the compositional space investigated, with Fe substituting for Mn on the Heusler lattice, with little or no antisite disorder. Despite the lack of chemical phase separation, magnetic phase separation is present in compositions near $x = 0.50$, where the coexistence of AFM and FM domains is confirmed by 15 K neutron diffraction. At these intermediate compositions a large increase in magnetic coercivity is observed, in excess of 1 kOe, attributed to local exchange interactions.

DOI: 10.1103/PhysRevB.94.094412

I. INTRODUCTION

Heusler compounds, with chemical formulas XY_2Z where X and Y are transition metals and Z is a main group element, have long been a popular system for scientific study due to the wide array of physical phenomena they express and their attendant technological applications. The most prominent [1,2] of these behaviors are those related to magnetism, many of which are central to spintronics applications, as conduction electrons in many XCo_2Z Heuslers are calculated by density functional theory (DFT) to be nearly 100% spin polarized [3,4].

Another aspect that makes magnetism in Heusler compounds (alternatively called "full-Heusler" to distinguish from the closely related XYZ half-Heusler crystal structure) interesting is that the magnetic behavior is closely related to the valence electron count (VEC) of the alloy. In addition to exhibiting Slater-Pauling behavior [5], in which the total magnetic moment in ferromagnetic (FM) compounds scales linearly with VEC, full-Heusler systems often transition between antiferromagnetic (AFM) and FM behavior with a change of atom on the X or Z site. This has been observed in particular in $(Mn,Fe)Ru_2Z$, where $MnRu_2Z$ compounds with Z = Si, Ge, Sn, or Sb are antiferromagnetic [5–8], while $FeRu_2Z$ with Z = Ge or Sn is ferromagnetic. ($FeRu_2Si$ is an antiferromagnet.)

Mizusaki *et al.* [9] explored the evolution of magnetic properties in $MnRu_2Ge$ as Fe is substituted onto the Mn site, $Mn_{1-x}Fe_xRu_2Ge$, observing a spike in magnetic coercivity at intermediate compositions between the antiferromagnetic $MnRu_2Ge$ and soft ferromagnetic $FeRu_2Ge$ with no evidence of phase separation. This AFM/FM chemical proximity allows for the study of exchange bias—a broadening and shifting of the magnetic hysteresis loop, understood to arise from the pinning of spins at the AFM/FM domain interface—in a solid solution, as opposed to more common exchange bias studies of AFM/FM nanocomposites [10–12] or thin films with planar interfaces [13].

In this communication we detail the magnetic behavior of $Mn_{1-x}Fe_xRu_2Sn$, a system in which the end-member Heusler compounds display magnetic ordering analogous to those of $(Mn,Fe)Ru_2Ge$. Similarly, we observe a large increase in magnetic coercivity, H_C, but no indication of phase separation

*jedouglas@mrl.ucsb.edu

into Mn- (AFM) and Fe-rich (FM) regions. Neutron and electron diffraction and spectroscopy of the (nominal) solid solution suggest multiple local environments for Fe, which may also influence the observed hysteresis.

II. EXPERIMENTAL METHODS

To explore the magnetic properties, seven compositions of $Mn_{1-x}Fe_xRu_2Sn$ were prepared through traditional solid-state routes, with $x = 0, 0.25, 0.40, 0.50, 0.60, 0.75$, and 1. Starting materials of elemental Mn, Fe, Ru, and Sn powders were mixed together by mortar and pestle, then heated in evacuated fused-silica ampoules at 1373 K for 1 h, followed by 18 h at 1173 K. The material was then reground before heating again at 1173 K, from which they were quenched into ice water after 168 h. A heating ramp of 5 K min^{-1} was used for all samples.

Structure and phases present were characterized in all samples by powder x-ray diffraction (XRD), acquired with a Philips X'Pert Powder Diffractometer with Cu $K\alpha$ radiation. Time-of-flight (TOF) neutron diffraction data was collected at 350 K for $x = 0$, 0.25, 0.50, 0.75, and 1 samples (and 15 K for $x = 0$, 0.50, and 1) using the NPDF instrument at the Los Alamos Neutron Science Center (LANSCE) of Los Alamos National Laboratory (LANL). Approximately 4 g of sample were measured in vanadium cans for between 2 h and 4 h. The nuclear and magnetic structure were analyzed by the Rietveld method, using a combination of the GSAS (EXPGUI interface) [14,15] and FullProf [16] software suites. Least-squares fitting of the real-space neutron pair distribution function (PDF) was performed with the PDFgui program [17], on data reduced using PDFgetN, $Q_{max} = 35$ Å^{-1}, to get the $G(r)$ function.

^{57}Fe Mössbauer spectroscopy was performed using a WissEl spectrometer which was operated in the constant acceleration mode and equipped with a ^{57}Co/Rh source. Spectra were collected on about 60 mg of sample for each composition (sans $MnRu_2Sn$) mixed with boron nitride, in an acrylic glass sample container 13 mm in diameter within a Janis SHI-850-5 closed cycle refrigerator. Data was collected at room temperature and 5 K. Select samples were also measured at 200 K. The data was analyzed with the program MossWinn [18] within the thin absorber approximation. Hyperfine field distributions were extracted using the modified Hesse method implemented in MossWinn. All isomer shifts are given versus α-Fe.

Magnetic properties were measured using a Quantum Design 5XL MPMS SQUID magnetometer. For "zero-field cooled" (ZFC) magnetization, M, versus temperature, T, measurements, samples were cooled from 400 K in the absence of a magnetic field, H, then M measured upon heating with a field of 100 Oe or 1 kOe ($x = 0.40$ and 0.50 samples). The "field cooled" (FC) M is measured upon cooling. The magnetization versus field, M vs H, was measured between +50 kOe and −50 kOe (±5 T) at 4 K and 300 K, mounted in wax to impede reorientation of the crystallites in response to the field. Curie temperatures for the $x = 0.75$ and 1 were measured using the electromagnet option on a TA Discovery thermo-gravimetric analyzer (TGA), as they order above the measurement range of the 5XL MPMPS.

Scanning electron microscopy (SEM) was performed on powders mounted on carbon tape, using an FEI XL30 Sirion FEG microscope, equipped with a backscattered-electron (BSE) detector. Transmission electron microscopy was performed on the FEI Tecnai T20 microscope, using lamellae prepared by focused-ion beam milling. Spin-polarized density functional theory (DFT) calculations were performed on $MnRu_2Sn$ and $FeRu_2Sn$, utilizing the Vienna *ab-initio* Software Package (VASP) [19]. The Perdew-Burke-Ernzerhof generalized gradient approximation (GGA-PBE) was used to describe exchange and correlation, within the projector augmented wave method (PAW) [20,21].

III. AVERAGE PROPERTIES

A. Phase and structure

Both $MnRu_2Sn$ and $FeRu_2Sn$ form in the Heusler crystal structure ($L2_1$, space group $Fm\bar{3}m$). The two share very similar lattice parameters, approximately 0.3% larger in the Mn compound than the Fe analog, with the former being AFM whereas the latter is FM. A principal question in the intermediate $Mn_{1-x}Fe_xRu_2Sn$ then is whether there is a solid solution between Mn and Fe on the 4*a* (000) Wyckoff position or if the two separate regionally, either into the end-member compositions or into intermediate phases. For this purpose x-ray and neutron powder diffraction data were taken of the materials and analyzed by Rietveld refinement. Fe and Mn have little contrast in x-ray scattering but very different neutron scattering lengths [22], which makes neutrons particularly useful in allowing for chemical determination in these materials. As such, our discussion is limited to the neutron diffraction patterns of $x = 0$, 0.25, 0.50, 0.75, and 1 samples.

Shown in Fig. 1(a) is a representative fit of 350 K neutron diffraction data. There is no peak splitting suggestive of Heusler phase separation in any of the diffraction patterns. The absence of phase separation on the Mn/Fe sublattice is also supported by Rietveld refinement. First, when two Heusler phases are used to model the data they refine to equal lattice parameters. Second, the refined lattice parameters, Fig. 1(b), follow the Vegard law, decreasing in a linear fashion with Fe concentration, from 6.215 Å in $MnRu_2Sn$ to 6.198 Å in $FeRu_2Sn$.

The refined Mn:Fe ratio of the Heusler phase from neutron diffraction matches closely with the nominal loading, as does that measured by large-area SEM EDX scans, Fig. 2(a). More local SEM or TEM EDX measurements—a line scan of the former is shown in Fig. 2(b)—gave no evidence of spatial variation of the Mn:Fe ratio that might suggest $MnRu_2Sn/FeRu_2Sn$ phase separation. By EDX there is a bit less Ru (and more Sn) than expected within the Heusler phase, as confirmed by selected-area diffraction patterns (SADP). This concurs with our Rietveld fits, which do show slightly smaller R_{wp} when Sn occupancy is allowed on the Ru site—the $Mn_{0.50}Fe_{0.50}Ru_2Sn$ data refines to $Mn_{12.2}Fe_{12.8}Ru_{45.3}Sn_{29.7}$, for example. (Compare average at. % values in Fig. 2.) Although these deviations from stoichiometry are minor and could be considered within error for neutron diffraction and EDX alone, we believe the combination of the two techniques supports Sn substitution on the Ru site.

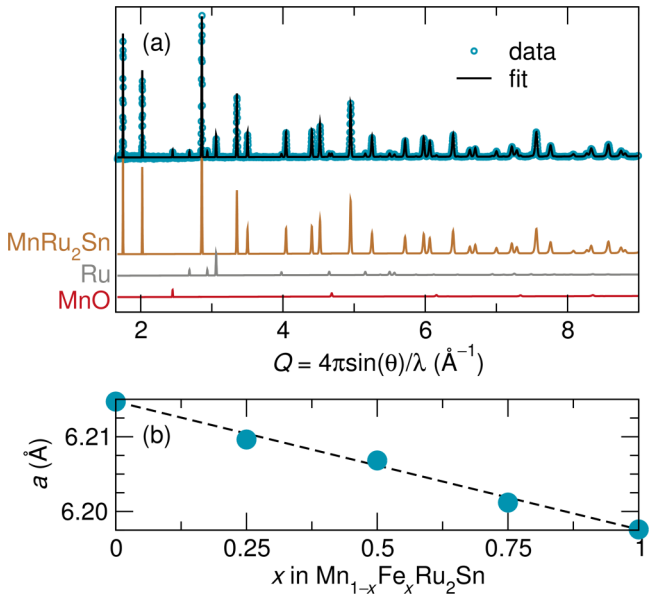

FIG. 1. (a) Rietveld refinement of powder neutron diffraction data for $x = 0$ sample in $Mn_{1-x}Fe_xRu_2Sn$ at 350 K. The contributions from each phase are decomposed beneath. This is the only composition for which MnO peaks are observed. (b) Refined lattice parameter, a, of the Heusler phase in $Mn_{1-x}Fe_xRu_2Sn$.

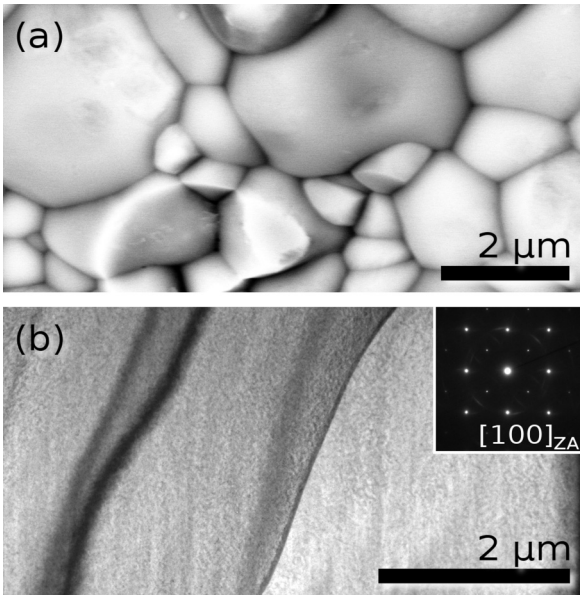

FIG. 3. (a) Scanning electron microscopy, imaged using the backscattered electron detector, and (b) transmission electron microscopy, including SADP, of $Mn_{0.50}Fe_{0.50}Ru_2Sn$. No chemical separation of Mn and Fe was observed in SEM or TEM EDX line scans, the former of which is displayed in Fig. 2. The diagonal line near the center of (b) is a grain boundary, while the broader two to the left are bend contours.

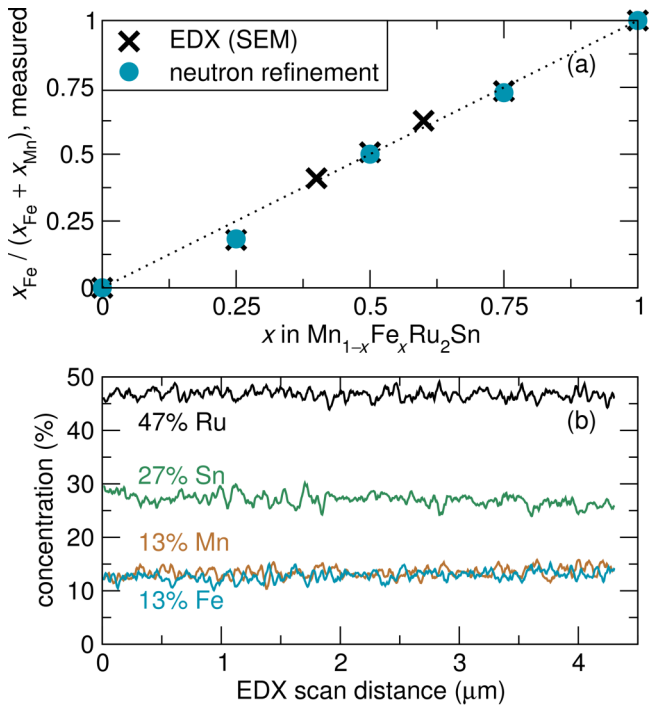

FIG. 2. (a) Concentration of Fe, x_{Fe}, as a function of weighed composition x, from both SEM energy-dispersive x-ray spectroscopy (EDX) and Rietveld refinement of neutron data. (b) Elemental concentrations from a representative EDX line scan of $Mn_{0.50}Fe_{0.50}Ru_2Sn$, overlaid on the micrograph. There is no spatial variation of Mn:Fe ratio.

Additionally, in all of the samples a Ru minor phase was detected by powder diffraction, which would account for the Ru deficiency of the Heusler phase. Using the XRD data the hexagonal close-packed (HCP) Ru phase refines to approximately 5% mole fraction by Rietveld refinement. Given that HCP Ru accepts a large solubility of Fe [23] and Mn [24], this HCP impurity is likely to be some Ru-rich solid solution of (Ru,Mn,Fe); however, no ternary phase diagram has been published. The correlation between scattering strength and mole-fraction of different elements in a structure with a single Wyckoff site makes it difficult to determine the composition of this HCP phase solely by refinement of the neutron data. Figure 3 shows micrographs representative of our SEM and TEM experiments in which neither Z contrast nor crystallite morphology evinced the HCP phase. This microscopy was largely hampered by the fact it was undertaken on powder surfaces; more detailed metallographic studies on polished material would be needed to visualize the phase distribution. As such we were unable to use a spatial probe such as EDX for chemical analysis of this phase specifically. For one sample only, the $MnRu_2Sn$ material, diffraction peaks from the AFM distorted rocksalt MnO are also present, and TEM shows the presence of MnO nanoprecipitates at many of the Heusler grain triple points.

By analyzing the 15 K neutron diffraction patterns of these materials, we are also able to gather information about the magnetic ordering from neutron interaction with the electron spin. The 15 K patterns for $x = 0$, 0.50, and 1 are presented in Fig. 4. The Fe-only sample, which orders ferromagnetically, shows no additional peaks from the 350 K pattern. The

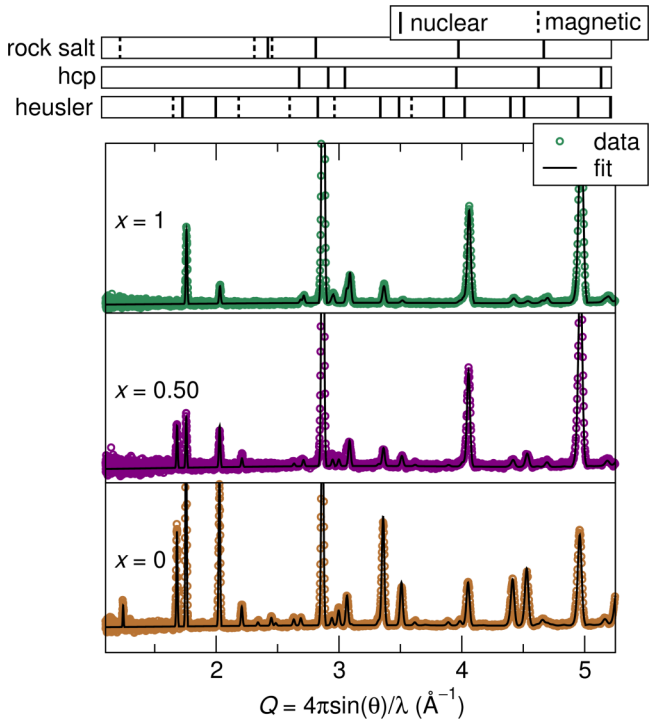

FIG. 4. 15 K powder neutron diffraction of $Mn_{1-x}Fe_xRu_2Sn$. $FeRu_2Sn$ shows only the Heusler nuclear peaks and HCP Ru impurity. In addition to these peaks, at $x = 0.50$ magnetic ordering peaks associated with (111) AFM order in the Heusler appear. The $x = 0$ material has all of these peaks as well as the nuclear and AFM peaks of rocksalt MnO.

Mn-only pattern, by comparison, has a number of peaks that arise due to the magnetic symmetry in each of two phases (see the Appendix) below their Néel temperatures, T_N: (i) the $MnRu_2Sn$, in which ferromagnetic (111) planes of Mn alternate between the moments pointing up and down normal to the plane [6], and (ii) the similar AFM ordering in MnO of alternating FM-coupled (111) planes, but with the moments pointing (approximately) in the plane [25].

The refined magnetic moments in $FeRu_2Sn$ at 15 K are 3.16(4) μ_B for Fe and 0.4(1) μ_B for Ru. These values correspond well to those calculated by DFT of 3.12 μ_B for Fe and 0.5 μ_B for Ru, and total moment, 4 μ_B, matches that predicted by Slater-Pauling: the VEC, 28, minus 24 [5]. For $MnRu_2Sn$ the refinement gives a moment only for Mn, 3.4(1) μ_B, slightly greater than the 3.27 μ_B we calculate from DFT.

Most notably, the 50:50 sample also shows Heusler (111) AFM ordering in addition to the nuclear peaks. The presence of AFM ordering at the composition is notable as the magnetization, M, versus magnetic field, H, is FM in nature, with a considerably larger coercivity, H_c, than $FeRu_2Sn$. Despite the lack of evidence for chemical phase separation between $MnRu_2Sn$ and $FeRu_2Sn$, either by diffraction or electron microscopy, the new peaks at 15 K suggest that there is some *magnetic* phase separation causing the increase in H_c.

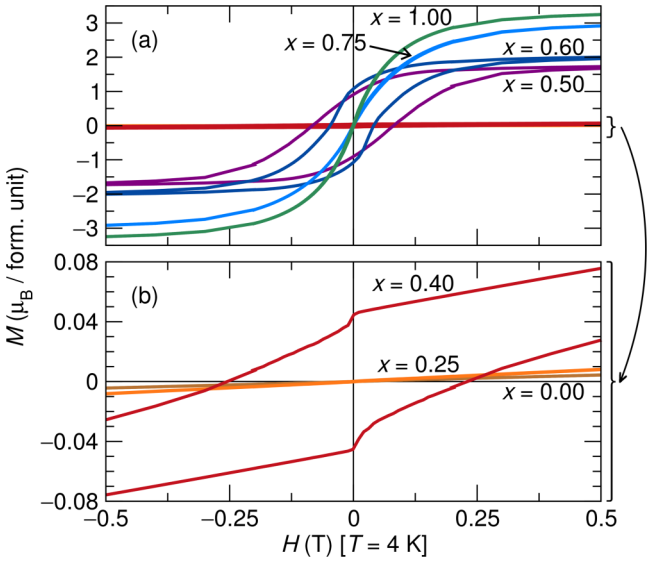

FIG. 5. Magnetization, M, as a function of magnetic field, H, for $Mn_{1-x}Fe_xRu_2Sn$ at 4 K.

B. Magnetic properties

As shown in Fig. 5, while the Mn and Fe end members display classic AFM and soft-FM behavior, respectively, intermediate compositions show a widening of the hysteresis loop, displaying chiefly FM behavior in which the Fe occupancy of the X site is at least 50% (i.e., $x \geqslant 0.50$). Below this concentration, the behavior is chiefly antiferromagnetic, though there is some hysteresis in the $Mn_{0.60}Fe_{0.40}Ru_2Sn$ sample, giving it a coercivity of approximately 2.5 kOe.

There are also features in the susceptibility data, χ versus T, that suggest the presence of coexisting AFM and FM ordering at intermediate compositions. (See Fig. 6.) The magnetization of the $x = 0.60$ sample mainly resembles FM behavior with

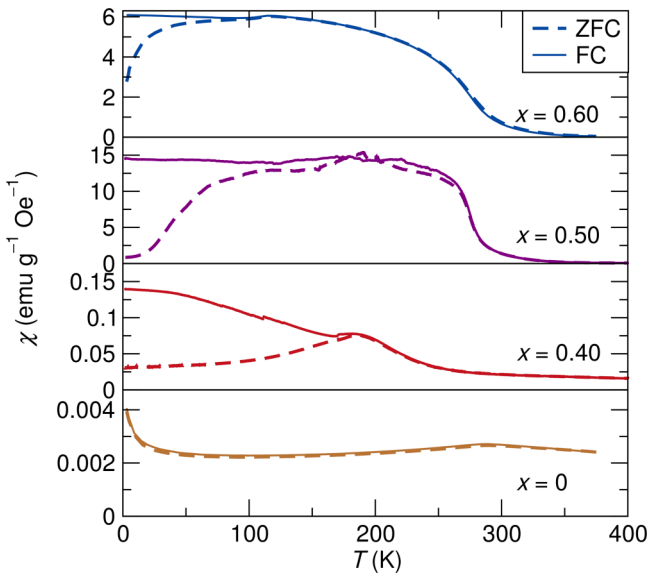

FIG. 6. Magnetic susceptibility, χ, as a function of temperature for $Mn_{1-x}Fe_xRu_2Sn$. $x = 0$ and 0.60 were measured under a field of 100 Oe, while $x = 0.40$ and 0.50 were measured at 1 kOe.

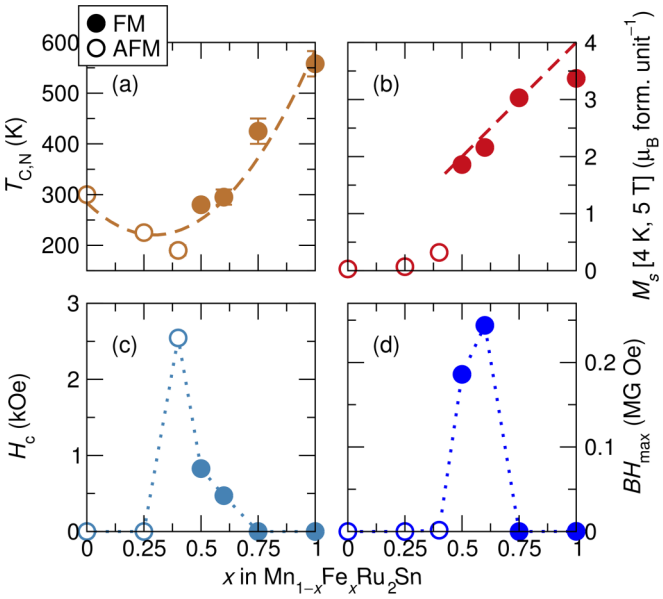

FIG. 7. Magnetic properties versus composition. (a) Magnetic ordering temperature, T_N or T_C. (b) Magnetization, M_s, at 5 T and 4 K. (c) Coercivity, H_c, at 4 K. (d) Magnetic energy product, BH_{max}, at 4 K.

a Curie temperature, T_C, just below 300 K, but shows a small AFM peak at 119 K. The $x = 0.40$ material shows a (broad) peak at the T_N of 190 K, but χ continues to rise upon field cooling, indicating more cooperative ordering of the spins. [The large "background" magnetization observed in $MnRu_2Sn$ is likely due to contribution from the paramagnetic HCP (Ru,Mn,Fe) impurity.]

Examining the magnetic ordering temperatures as a function of composition, Fig. 7(a), we see that even the $T_{C,N}$ of the dominant ordering—AFM or FM—of the material is suppressed by a mixture of Fe and Mn at the X site, as the long-range exchange interactions are weaker in the statistical distribution of Mn/Fe than the pure end-member compounds. This is true to an even greater degree for the minor ordering, which occurs at much lower T than the dominant if it occurs at all.

The trend of saturation magnetization (i.e., M at 5 T), M_s, as a function of composition illustrates this weakened interaction as well. The measured values are plotted in Fig. 7(b). The $x = 1$ sample has an M_s of approximately 3.4 μ_B per formula unit, falling short of the 4 μ_B calculated by neutron diffraction and DFT likely because the material is not single-phase Heusler. From this value the magnetization decreases approximately linearly with Fe concentration through $x = 0.50$, after which M_s collapses nearly to zero upon the material becoming Mn rich. In this range local concentrations of Fe are no longer able to order ferromagnetically to a macroscopically meaningful extent.

The H_c at each composition is plotted in Fig. 7(c). However, as evidenced by the $x = 0.40$ sample, where H_c is 2.5 kOe only by dint of its characteristic low AFM slope, the maximum energy product, BH_{max}, Fig. 7(d), is a better measure of increased hardness. By this measure, the effect peaks at $Mn_{0.40}Fe_{0.60}Ru_2Sn$, with a similar value at the 50:50 composition. For every other composition, BH_{max} is essentially zero.

While there was a significant increase in H_c, we observe no shifting of the hysteresis loop when cooled from above T_N under a field of 50 kOe. Therefore, the increased magnetization energy is not caused by a prototypical "exchange bias" effect but by a more local competition of AFM and FM exchange.

IV. LOCAL PROPERTIES

The average structure as determined by Rietveld refinement of neutron (and x-ray) diffraction gives no indication that there is phase separation between $MnRu_2Sn$ and $FeRu_2Sn$ in the intermediate compositions of $Mn_{1-x}Fe_xRu_2Sn$. On the other hand, the magnetic behavior of these materials, specifically the increase in H_c and the low-temperature neutron diffraction, are emblematic of combined AFM and FM orderings in the material, states associated with the two end-member compounds. To substantiate a lack of chemical phase separation despite this latter fact, techniques were pursued to study the local environment in these materials.

A. Local structure

To explore local correlations in these compounds, the pair distribution function (PDF) was acquired by transforming the reciprocal space neutron scattering data into a real space $G(r)$, analyzed above $T_{C,N}$ to avoid contributions of magnetism to the data. Representative 350 K PDFs—for the end-member compounds and $Mn_{0.50}Fe_{0.50}Ru_2Sn$—in the range of 2 Å to 5 Å are shown in Fig. 8.

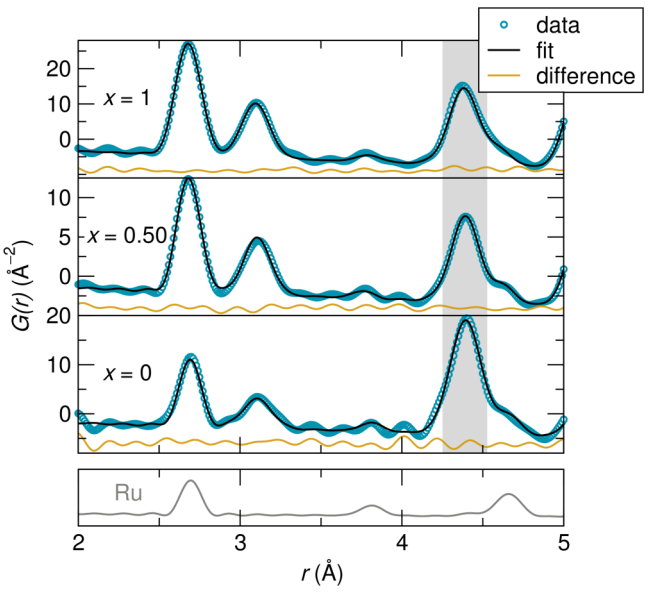

FIG. 8. Neutron pair distribution function, $G(r)$, of $Mn_{1-x}Fe_xRu_2Sn$, transformed from 350 K neutron scattering data. The data is well modeled by the average structure as a solid solution. There is no observed splitting of the third coordination shell (gray region, ≈4.4 Å), which corresponds to the nearest (Mn,Fe)–(Mn,Fe) pair. The contribution of the Ru phase to the PDF is shown beneath, scaled up for clarity.

There is little qualitative difference between the PDFs of these three compounds. Specifically, if there were a proclivity for Mn (and thereby Fe) atoms to cluster locally, it is expected that there would be a broadening or splitting of the shortest (Mn,Fe)-Sn correlation peak, ≈3.1 Å, or (Mn,Fe)-(Mn,Fe) peak, ≈4.4 Å. However, no such splitting is observed, nor are the atomic displacement parameters, U_{iso}, for the X (Mn,Fe) site unusually large. The PDF in a range of 1.5 Å to 30 Å (not shown) is also well described by the Heusler average structure obtained by Rietveld refinement.

Regarding the impurity "HCP" phase, there is some indication that the phase is locally distorted, with fits in the range of $r \leqslant 5$ Å being best described by a *Pnma* symmetry, corresponding to a reduction of the c/a ratio. This is possibly due to a need to accommodate this (Ru,Mn,Fe) phase coherently with the Heusler lattice.

B. Mössbauer spectroscopy

A fitting complement to neutron PDF is Mössbauer spectroscopy, as it is similarly a probe of the local environment in the crystal and furthermore sensitive to the local magnetic order. $Mn_{1-x}Fe_xRu_2Sn$ is particularly well suited for Mössbauer as it contains several Mössbauer active elements (Fe, Ru, and Sn), and its magnetic order/disorder transitions can be followed over accessible temperature regimes. Here we performed ^{57}Fe Mössbauer spectroscopy on the $Mn_{1-x}Fe_xRu_2Sn$ materials to further characterize the type of phases present, the local atomic order, and the local magnetic properties.

Representative Mössbauer spectra are shown in Fig. 9. Magnetically ordered phases are indicated by a six-line pattern, which captures the hyperfine splitting due to local magnetic fields, whereas magnetically disordered phases give rise to singlet components. When measured at room temperature [292 K, Fig. 9(a)] only the $x = 1$ and 0.75 samples have a sextet contribution. All lower Fe loadings show only a broadened single line like in the $Mn_{0.40}Fe_{0.60}Ru_2Sn$ spectrum. The evolution of the spectral shape with x at 292 K reflects the fact that the magnetic ordering temperature decreases with decreasing Fe content. In the case of $x \leqslant 0.60$, this temperature is below 292 K. The systematic change in the spectra again refutes the idea of extensive Fe clustering (at the X site): considering that the Curie temperature, T_C, of $Mn_{1-x}Fe_xRu_2Sn$ is 593 K [26], it is expected that local pockets of $FeRu_2Sn$ would still exhibit hyperfine splitting at room temperature, but this is not observed even at a concentration of $x = 0.60$.

At 5 K, on the other hand, all compositions show absorption lines from both a majority sextet and a minority singlet component. The isomer shifts δ and hyperfine fields H_{hf} obtained from the evaluation of the 5 K spectra are summarized in Table I. Strain and disorder effects are always present which cause broadened absorption lines; as such the spectra were fit using a hyperfine field distribution model rather than a single sextet. As seen in Fig. 9(b), the average hyperfine field, H_{hf}, of the sextet pattern increases upon cooling from room temperature, which reflects the increasing degree of magnetization of the sample. The very broad pattern at 200 K suggests that due to atomic disorder rather a distribution of transition temperatures occurs.

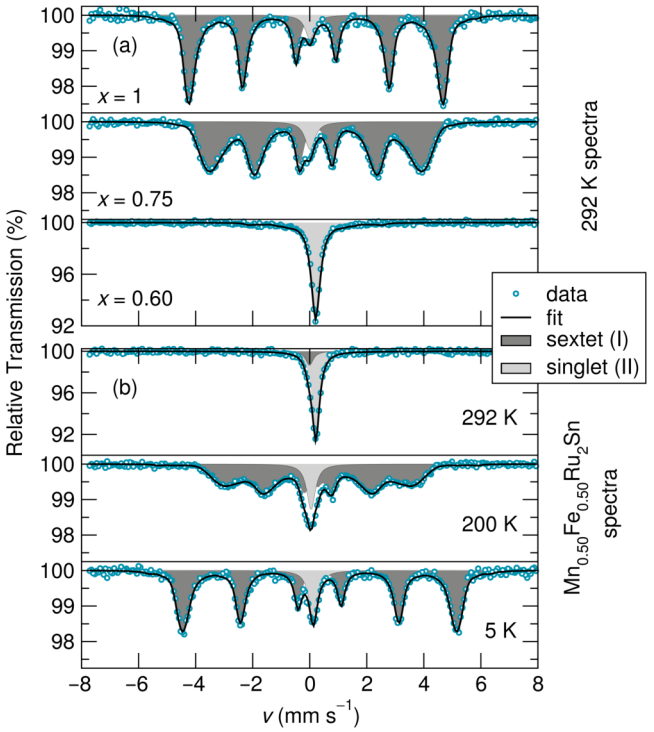

FIG. 9. Representative ^{57}Fe Mössbauer spectra of $Mn_{1-x}Fe_xRu_2Sn$, both (a) room temperature measurements at multiple compositions and (b) $Mn_{0.50}Fe_{0.50}Ru_2Sn$ spectra at multiple temperatures. All samples with compositions of $x < 0.75$ show room-temperature spectra equivalent to that of $x = 0.60$.

The presence of only a single hyperfine sextet component at low temperatures is consistent with the spectra observed for the related stoichiometric $L2_1$-type Heusler phases $FeCo_2Z$ [27], where the Fe atoms reside entirely on the octahedral ($4a$) sites. By contrast when Fe occurs on both the X and Y sites, either through substitution for Co atoms on the $8c$ site ($Fe_{1+x}Co_{2-x}Z$) [28,29] or in a stoichiometric XFe_2Z inverse Heusler compound [30], two hyperfine sextet in components with considerably different H_{hf} are observed, reflecting the difference in magnetic moment at each of the crystallographic sites. The absence of a second sextet here as well as the

TABLE I. Hyperfine magnetic field, H_{hf} (peaks of the distribution), isomer shifts, δ, and area fractions (A) of the two subspectra measured by Mössbauer spectra at 5 K. Subspectrum I corresponds to Fe in the octahedral site of the $L2_1$ Heusler phase (sextet in Fig. 9). Subspectrum II is paramagnetic Fe, most likely within an HCP impurity phase (singlet).

x $Mn_{1-x}Fe_xRu_2Sn$	H_{hf}(I) (T)	δ(I) (mm/s)	A(I) (%)	H_{hf}(II) (T)	δ(II) (mm/s)	A(II) (%)
1	31.6	0.347	95	...	0.110	5
0.75	31.1	0.344	93	...	0.135	7
0.60	29.9	0.344	98	...	0.120	2
0.50	29.9	0.349	87	...	0.131	13
0.40	27.7	0.334	98	...	0.127	2
0.25	27.6	0.341	93	...	0.168	7

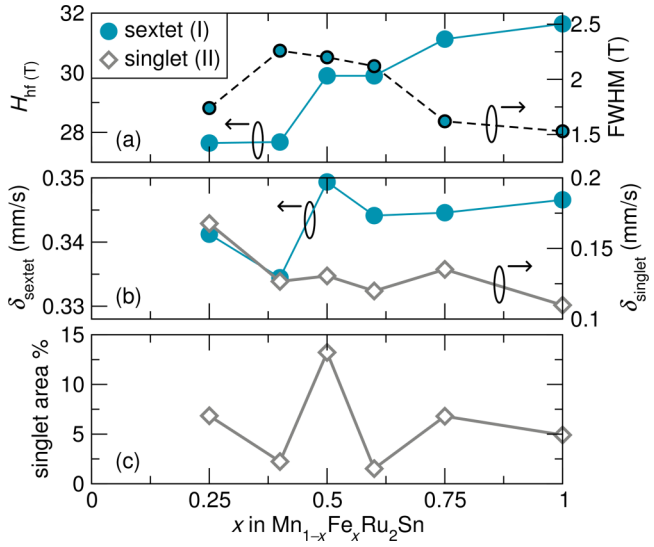

FIG. 10. ^{57}Fe Mössbauer parameters for $Mn_{1-x}Fe_xRu_2Sn$ as obtained at 5 K. (a) Peak hyperfine field, H_{hf}, and the full width half maximum (FWHM) for the hyperfine field distribution for the sextet absorption lines. (b) Isomer shift, δ, for the sextet and singlet. (c) Singlet area fraction.

large H_{hf} values of 28 T to 32 T indicate that there is negligible antisite disorder in the present system between Fe and Ru atoms (i.e., no $D0_3$-type disorder). For stoichiometric $FeRu_2Sn$ $H_{hf} = 31.6$ T, which agrees very well with values previously reported in literature, both for this compound [31,32] and the related Heusler compounds $FeCo_2Al$ [33] and $FeCo_2Si$ [28]. Compared to the 3.2 μ_B obtained from neutron data refinements discussed above for $FeRu_2Sn$, the Fe-site magnetic moment in $FeCo_2Al$ is 3 μ_B by DFT, whereas it is measured to be ~2.5 μ_B in $FeCo_2Si$ [34,35].

As shown in Fig. 10(a), the H_{hf} decreases monotonically with Fe content, which suggests a correspondent weakening of the magnetism at the Fe sites. In particular the change in H_{hf} is most pronounced between $x = 0.5$ and $x = 0.4$, the same range at which the transition from FM to AFM behavior is observed. The Fe atoms are fully magnetically ordered and contribute to the magnetic structure even at lower x concentrations; however, the type of spin ordering cannot be derived directly from zero-field Mössbauer spectra. The width of the hyperfine field distribution determined from modeling the sextet absorption lines peaks near $x = 0.5$. This is consistent with the scenario of magnetic phase separation, the absorption lines broadening due to the coexistence of an AFM and FM phase with slightly different H_{hf} values. This is also the composition range in which Mn/Fe disorder in the third coordination shell is most pronounced. Overall the isomer shift, δ, of the sextet component does not vary much with x, which indicates that the local electronic properties at the Fe sites remain largely unaffected by the consecutive replacement of Fe atoms by Mn atoms.

Finally we consider the broadened singlet peak discernible in all of the magnetically ordered samples, i.e., all 5 K spectra and the room-temperature spectra of $x = 0.75$ and 1. Its isomer shift is much smaller than that of the sextet component, and furthermore its area fraction varies between 2% and 13% with

TABLE II. Details from Rietveld refinement of 350 K neutron diffraction data, presented in Fig. 1(a).

$x = 0$, $R_{wp} = 7.1\%$			
Phase	Heusler	Ru	MnO
Nuclear Space Group	$Fm\bar{3}m$	$P6_3/mmc$	$Fm\bar{3}m$
a (Å)	6.21469(2)	2.7014(2)	4.4440(2)
c (Å)		4.2787(4)	

no discernible pattern as a function of x. Accordingly, it is most likely that the singlet corresponds to Fe residing in the HCP Ru phase seen in the diffraction data. While we are unaware of ^{57}Fe Mössbauer characterization of the full Ru–Fe solid solution, the isomer shift values of about 0.0 mm/s at room temperature are compatible with the data of Pearson *et al.* [36]. While Fe-rich HCP (Ru,Fe) is AFM, it behaves paramagnetically [23] at low Fe concentrations, hence the absence of hyperfine splitting here, and should not greatly influence the bulk magnetic properties.

V. CONCLUSIONS

In Heusler materials of the composition $Mn_{1-x}Fe_xRu_2Sn$, prepared by standard solid-state methods, we observe hard magnetic behavior at intermediate compositions between the AFM $MnRu_2Sn$ and FM $FeRu_2Sn$ end members. Whereas $FeRu_2Sn$ has a coercivity less than 10 Oe, the coercivity of $Mn_{0.50}Fe_{0.50}Ru_2Sn$, a hard ferromagnet, approaches 1 kOe

TABLE III. Details from Rietveld refinement of 15 K neutron diffraction data, presented in Fig. 4.

$x = 0$, $R_{wp} = 5.8\%$			
Phase	Heusler	Ru	MnO
Nuclear Space Group	$Fm\bar{3}m$	$P6_3/mmc$	$C2$
AFM Space Group	$R\bar{3}m'$		$C21'$
a (Å)	6.2009(1)	2.69723(9)	5.444(1)
b (Å)			3.1508(8)
c (Å)		4.2698(2)	15.168(3)
β (deg)			89.96(4)
Mn moment (μ_B)	3.4		4.5
$x = 0.50$, $R_{wp} = 6.2\%$			
Phase	Heusler	Ru	$Ru_{1-\delta}(Fe,Mn)_\delta$
Nuclear Space Group	$Fm\bar{3}m$	$P6_3/mmc$	$P6_3/mmc$
AFM Space Group	$R\bar{3}m'$		
a (Å)	6.1944(2)	2.6975(2)	2.6752(1)
c (Å)		4.2705(5)	4.2546(4)
AFM moment (μ_B)	3.2		
FM moment (μ_B)	2.3		
$x = 1$, $R_{wp} = 5.9\%$			
Phase	Heusler	Ru	$Ru_{1-\delta}Fe_\delta$
Nuclear Space Group	$Fm\bar{3}m$	$P6_3/mmc$	$P6_3/mmc$
a (Å)	6.1859(2)	2.6976(1)	2.67266(9)
c (Å)		4.2719(4)	4.2490(2)
Fe moment (μ_B)	3.2		
Ru moment (μ_B)	0.4		

TABLE IV. Details from least-squares modeling of 350 K neutron pair distribution function (NPDF) data, fit from 1.5 Å to 5 Å. Data and fits are presented in Fig. 8.

$x = 0$, $R_{wp} = 14.4\%$			
Phase	Heusler	Ru	MnO
Space Group	$Fm\bar{3}m$	$P6_3/mmc$	$Fm\bar{3}m$
a (Å)	6.217(2)	2.690(5)	4.41(2)
c (Å)		4.42(2)	
Mn U_{iso} (Å^2)	0.0054(6)		0.01(2)
Ru U_{iso}(Å^2)	0.0065(3)	0.0032(3)	
Sn U_{iso} (Å^2)	0.0056(3)		
O U_{iso} (Å^2)			0.0001(8)
$x = 0.50$, $R_{wp} = 7.9\%$			
Phase	Heusler	Ru	
Space Group	$Fm\bar{3}m$	$P6_3/mmc$	
a (Å)	6.2177(7)	2.684(2)	
c (Å)		4.256(9)	
Mn,Fe U_{iso} (Å^2)	0.005(1)		
Ru U_{iso}(Å^2)	0.0054(3)	0.0026(2)	
Sn U_{iso} (Å^2)	0.0028(2)		
$x = 1$, $R_{wp} = 7.3\%$			
Phase	Heusler	Ru	
Space Group	$Fm\bar{3}m$	$P6_3/mmc$	
a (Å)	6.1971(6)	2.630(3)	
c (Å)		4.55(1)	
Fe U_{iso} (Å^2)	0.00315(1)		
Ru U_{iso}(Å^2)	0.0078(2)	0.0047(3)	
Sn U_{iso} (Å^2)	0.0061(5)		

at 4 K. This increase occurs despite the lack of a chemical phase separation of $MnRu_2Sn$ and $FeRu_2Sn$, which would be expected under the commonly cited cause of magnetic hardening in AFM/FM composite materials due to exchange bias. Powder diffraction, PDF analysis, and ^{57}Fe Mössbauer spectroscopy all gave no evidence that Mn and Fe atoms were locally segregated on the Heusler lattice.

Powder neutron diffraction data of the $x = 0.50$ materials at 15 K, however, shows the presence of AFM ordering across the (111) planes of the Heusler material, through a number of magnetic diffraction peaks that are not present at 350 K. Therefore, while there is no *chemical* phase separation in the intermediate compositions, there appears to be a *magnetic* phase separation within the material. It is known from previous literature that this exchange bias behavior can occur in such a solid solution [37], due to more local exchange interactions between the atoms. However, this has not been as widely explored as in thin films or nanocomposites, in which the magnetic ordering and structural phase are (assumed to be) geometrically synonymous.

The tunability of Heusler compounds and chemical proximity of AFM and FM materials in this structure make them ideal for studying hardening in solid solution materials. A similar AFM/FM phase coexistence has been exploited recently in $Pt_xMn_{3-x}Ga$, leading to giant exchange bias in excess of 3 T [38]. Interestingly, in the half-Heusler solid solution $MnCu_{1-x}Ni_xSb$ [39], a mixed magnetic phase region exists at $0.05 \leqslant x \leqslant 0.2$ rather than centered around $x = 0.5$ like observed here in $Mn_{1-x}Fe_xRu_2Sn$ and in $Pt_xMn_{3-x}Ga$. Theoretical studies of the exchange interactions that lead to such differences in behavior would be insightful for controlling magnetism in these sorts of systems. Additionally, imaging these magnetic domains by advanced microscopy techniques would be important experimentally to develop our understanding.

ACKNOWLEDGMENTS

This work was supported by the MRSEC Program of the National Science Foundation through Grant No. DMR-1121053. J.E.D. is supported by the National Science Foundation Graduate Research Fellowship Program under Grant No. 1144085. J.E.D. acknowledges the support of Grant No. NSF 0843934 as well. The Materials Research Laboratory is a member of the NSF-supported Materials Research Facilities Network. C.F. acknowledges financial support by the ERC Advanced Grant No. 291472 "Idea Heusler." We thank Dr. Geneva Laurita for fruitful discussions of neutron scattering.

APPENDIX: DETAILS OF THE CRYSTAL STRUCTURES

Included here in Tables II–IV are pertinent details of the crystal structures as determined by fits to the neutron scattering data plotted in Figs. 1, 4, and 8.

[1] F. Heusler, Verhandl. Deut. Physik. Ges. **5**, 219 (1903).
[2] T. Graf, S. S. P. Parkin, and C. Felser, IEEE Trans. Magn. **47**, 367 (2011).
[3] S. Picozzi, A. Continenza, and A. J. Freeman, Phys. Rev. B **69**, 094423 (2004).
[4] F. Casper, T. Graf, S. Chadov, B. Balke, and C. Felser, Semicond. Sci. Technol. **27**, 063001 (2012).
[5] I. Galanakis, P. H. Dederichs, and N. Papanikolaou, Phys. Rev. B **66**, 174429 (2002).
[6] T. Kanomata, M. Kikuchi, and H. Yamauchi, J. Alloys Compd. **414**, 1 (2006).
[7] S. Ishida, S. Kashiwagi, S. Fujii, and S. Asano, Physica B: Condens. Matter **210**, 140 (1995).
[8] S. Khmelevskyi, E. Simon, and L. Szunyogh, Phys. Rev. B **91**, 094432 (2015).
[9] S. Mizusaki, A. Douzono, T. Ohnishi, T. C. Ozawa, H. Samata, Y. Noro, and Y. Nagata, J. Alloys Compd. **510**, 141 (2012).
[10] J. Nogués and I. K. Schuller, J. Magn. Magn. Mater. **192**, 203 (1999).
[11] Z. M. Tian, S. L. Yuan, L. Liu, S. Y. Yin, L. C. Jia, P. Li, S. X. Huo, and J. Q. Li, J. Phys. D: Appl. Phys. **42**, 035008 (2009).
[12] D. P. Shoemaker, M. Grossman, and R. Seshadri, J. Phys.: Condens. Matter **20**, 195219 (2008).

[13] K. O'Grady, L. E. Fernandez-Outon, and G. Vallejo-Fernandez, J. Magn. Magn. Mater. **322**, 883 (2010).
[14] A. C. Larson and R. B. Von Dreele, Los Alamos National Laboratory, Report LAUR 86, 2000 (unpublished).
[15] B. H. Toby, J. Appl. Crystallogr. **34**, 210 (2001).
[16] J. Rodríguez-Carvajal, Physica B **192**, 55 (1993).
[17] C. L. Farrow, P. Juhas, J. W. Liu, D. Bryndin, E. S. Božin, J. Bloch, T. Proffen, and S. J. L. Billinge, J. Phys.: Condens. Matter **19**, 335219 (2007).
[18] Z. Klencsár, E. Kuzmann, and A. Vértes, J. Radioanal. Nucl. Chem. **210**, 105 (1996).
[19] G. Kresse and J. Furthmüller, Comput. Mater. Sci. **6**, 15 (1996).
[20] G. Kresse, M. Marsman, and J. Furthmüller, Vienna Ab-Initio Simulation Package: VASP the GUIDE, 2012, http://cms.mpi.univie.ac.at/vasp/vasp/vasp.html.
[21] G. Kresse and D. Joubert, Phys. Rev. B **59**, 1758 (1999).
[22] V. F. Sears, Neutron News **3**, 26 (1992).
[23] H.-J. Moon, W. D. Kim, S.-J. Oh, J.-W. Park, J.-G. Park, E.-J. Cho, J. I. Lee, and H.-C. Ri, J. Korean Phys. Soc. **36**, 49 (2000).
[24] T. B. Massalski, *Binary Alloy Phase Diagrams* (ASM International, Materials Park, OH, 1986), pp. 1583.
[25] A. L. Goodwin, M. G. Tucker, M. T. Dove, and D. A. Keen, Phys. Rev. Lett. **96**, 047209 (2006).
[26] C. Mitros, S. Yehia, S. Kumar, S. Jha, M. DeMarco, D. Mitchell, G. M. Julian, and R. A. Dunlap, Hyperfine Interact. **34**, 419 (1987).
[27] N. K. Jaggi, K. R. P. M. Rao, A. K. Grover, L. C. Gupta, R. Vijayaraghavan, and L. K. Dang, Hyperfine Interact. **4**, 402 (1978).
[28] V. Ksenofontov, M. Wójcik, S. Wurmehl, H. Schneider, B. Balke, G. Jakob, and C. Felser, J. Appl. Phys. **107**, 09B106 (2010).
[29] V. Jung, B. Balke, G. H. Fecher, and C. Felser, Appl. Phys. Lett. **93**, 042507 (2008).
[30] T. Gasi, V. Ksenofontov, J. Kiss, S. Chadov, A. K. Nayak, M. Nicklas, J. Winterlik, M. Schwall, P. Klaer, P. Adler, and C. Felser, Phys. Rev. B **87**, 064411 (2013).
[31] R. G. Pillay, R. Nagarajan, and P. N. Tandon, J. Phys. Colloq. **40**, C2-218 (1979).
[32] A. K. Grover, R. G. Pillay, V. Nagarajan, and P. N. Tandon, Phys. Status Solidi B **98**, 495 (1980).
[33] V. Jung, G. H. Fecher, B. Balke, V. Ksenofontov, and C. Felser, J. Phys. D: Appl. Phys. **42**, 084007 (2009).
[34] V. Niculescu, J. I. Budnick, W. A. Hines, K. Raj, S. Pickart, and S. Skalski, Phys. Rev. B **19**, 452 (1979).
[35] S. Wurmehl, G. H. Fecher, H. C. Kandpal, V. Ksenofontov, H.-J. Lin, and C. Felser, Appl. Phys. Lett. **88**, 032503 (2006).
[36] D. I. C. Pearson and J. M. Williams, J. Phys. F: Met. Phys. **9**, 1797 (1979).
[37] D. P. Shoemaker, E. E. Rodriguez, R. Seshadri, I. S. Abumohor, and T. Proffen, Phys. Rev. B **80**, 144422 (2009).
[38] A. K. Nayak, M. Nicklas, S. Chadov, P. Khuntia, C. Shekhar, A. Kalache, M. Baenitz, Y. Skourski, V. K. Guduru, A. Puri, U. Zeitler, J. M. D. Coey, and C. Felser, Nat. Mater. **14**, 679 (2015).
[39] M. Halder, S. M. Yusuf, A. Kumar, A. K. Nigam, and L. Keller, Phys. Rev. B **84**, 094435 (2011).